Materials Today Communications 37 (2023) 107028

Contents lists available at ScienceDirect

Materials Today Communications

journal homepage: www.elsevier.com/locate/mtcomm

CEBs with GRC: Fabrication, characterization, modeling, and correlation with microstructural fracture features

Marian Valenzuela [a], Jorge Leiva [b], Alexis Salas [c], Gustavo Ciudad [d,e,f], Juan Pablo Cárdenas [g], Angelo Oñate [h,j], Renato Hunter [b], Shady Attia [i], Víctor Tuninetti [b,*]

[a] Doctoral Program in Sciences of Natural Resources, Universidad de La Frontera, Casilla 54-D, Temuco 4780000, Chile
[b] Department of Mechanical Engineering, Universidad de La Frontera, Temuco 4780000, Chile
[c] Department of Mechanical Engineering (DIM), Faculty of Engineering, University of Concepción, 219 Edmundo Larenas, Concepción 4070409, Chile
[d] Scientific and Technological Bioresources Nucleus (BIOREN), Universidad de La Frontera, Avenida Francisco Salazar #01145, Casilla 54-D, Temuco 4780000, Chile
[e] Instituto del Medio Ambiente (IMA), Universidad de La Frontera, Avenida Francisco Salazar #01145, Casilla 54-D, Temuco 4780000, Chile
[f] Department of Chemical Engineering, Faculty of Engineering and Sciences, Universidad de La Frontera, Avenida Francisco Salazar #01145, Casilla 54-D, Temuco 4780000, Chile
[g] Department of Construction Engineering, Universidad Autónoma, Avenida Alemania #1090, Temuco 4780000, Chile
[h] Departamento de Ingeniería Mecánica, Facultad de Ingeniería, Universidad del Bío-Bío, 4051381 Concepción, Chile
[i] Department of Sustainable Building Design Lab, Dept. UEE, Faculty of Applied Science, University of Liege, Liege, Belgium
[j] Department of Materials Engineering, Universidad de Concepción, Concepción 4030000, Chile

ARTICLE INFO

Keywords:
CEB
Compressive strength
Three-point flexural strength
Material modeling

ABSTRACT

In this study, earth blocks (EB) and compressed earth blocks (CEB) are fabricated and investigated along with the development of a mathematical model of compressive and tensile loads. The investigated specimens are manufactured from a mixture of soil, ground recycled concrete (GRC) powder and water in weight fractions of 4:1:1. EBs are molded and CEBs are obtained by quasi-static compression in wet state. Material samples extracted from the blocks are tested in dry state for compressive strength and three-point flexural strength according to ASTM standards. The results indicate that CEB exhibits 130% higher compressive load capacity and 63% higher tensile strength compared to EB. Furthermore, the proposed and calibrated mathematical model is able to adequately describe the strength and damage behavior of both materials. Finally, microstructural/micromechanical interrelationships with the modeled material response are established based on a characterization of postmortem CEB samples using EDS elemental analysis and SEM micrographs techniques.

1. Introduction

In the last few years, there has been a renewed interest in earthen construction, particularly in the technological advancement of the compressed earth block technique. Compressed earth blocks (CEB) are manufactured by compacting a mixture of soil with water and other materials in smaller proportions to form a solid block. More sustainable and environmentally friendly measures have been adopted in the field of construction, such as the reuse of biodegradable materials in the manufacture of CEBs using waste or stabilizing by-products obtained from the agricultural, livestock and general industrial residues [1–4].

According to the scientific literature, the mechanical behavior of CEB depends on several parameters: some derived from the material itself, such as the composition, properties and particle size distribution of the soil, stabilizer, fibers or additives; while others are from the manufacturing variables such as the compaction mode, curing time, shape and dimensions of the block [5–8]. The resulting packing density of the mixture, directly correlated with void density fraction, explains the strength variation of earth based materials. Applying the packing particle theory, some authors have reported to determine the optimal particle size distribution for manufacturing CEB [9]. However, the strength of CEBs is still largely dependent on soil particle compaction and stabilizer application [9–11].

Overall, a CEB with adequate mechanical behavior is considered sustainable and cost-effective because soil is an abundant and readily available natural resource, with low cost and lower carbon footprint compared to conventional building elements. In addition, the use of CEBs instead of other construction elements such as concrete blocks or

* Corresponding author.
E-mail address: victor.tuninetti@ufrontera.cl (V. Tuninetti).

https://doi.org/10.1016/j.mtcomm.2023.107028
Received 14 May 2023; Received in revised form 6 August 2023; Accepted 1 September 2023
Available online 3 September 2023

fired bricks reduces manufacturing cost, energy and environmental impact [12]. Since CEBs require the use of local soil for their production, together with their known low capacity to withstand applied loads, their strength and performance to compression and tension must be particularly determined. A comprehensive study of mechanical properties of quasi-fragile materials is generally carried out using various experimental techniques, such as uniaxial compression test, biaxial compression test, bending test (three or four point), uniaxial tensile, direct shear and even with indentation testing. There are different standards for testing CEBs depending on the research and country of potential application [4], with the compressive response identified as being of most interest by researchers. As for the tensile response, it can be obtained directly by uniaxial testing or indirectly by flexural testing. These tests allow the determination of different material parameters such modulus of elasticity, yield point, strength, fracture strain, among others. The identification of these parameters constitutes the mathematical models that describe the mechanical behavior of a quasi-fragile material, which can be further integrated in a computational tool to simulate the construction element in a building structure.

Natural stabilizers, agro-industrial wastes or industry by-products incorporated into the compressed earth blocks modify the durability, strength, permeability, porosity, density and cohesion properties of the CEBs [13–18]. Fine materials act as binders while manufacturing compaction primarily contributes to improve cohesion of the CEBs in the wet state. In our work, fine soil and ground recycled concrete are assessed as binders and the compaction of mixtures is applied to quantify the strength improvement of CEB compared to EB.

Much research remains to be done to understand and optimize the use of ground recycled concrete as a binder in compressed earth blocks, since most of the work focuses on mortars and concrete manufacturing [19–23]. In this paper we focus on the ability of CEB to contain a considerable proportion of GRC evaluated in responses to damage-producing loads.

The two main objectives of this research are: (a) to report the manufacturing achievement of a novel compressed earth block (CEB) containing ground recycled concrete (GRC), with superior properties to earth block (EB) in terms of response to experimental tests of uniaxial compression and three-point bending loads; and (b) to propose and calibrate a mathematical model that simulates the macromechanical response for the observed stress-strain and hardening/softening behavior. Additionally, the microstructural characteristics of the fabricated and post-deformed CEBs are evaluated by SEM-EDS techniques, in order to identify and analyze the microstructural differences and the micromechanical damage and fracture mechanisms providing a roadmap to pursue the strength improvement of CEBs.

2. Materials and methods

2.1. CEBs manufacturing

The constituent raw materials of the CEBs used in this research include soil of maximum grain size of 0.525 mm, ground recycled concrete powder of 0.074 mm and neutral water (Fig. 1). The GRC particle size is comparable with those added in other previous studies [24,25]. According to ASTM, the soil is considered as fine to medium sand. Neutral water is selected as sulphate-rich water is known to destroy the hardened hydraulic binding matrix and increase the moisture sensitivity of the block. In addition, water containing organic matter and salt water can cause efflorescence. A suitable percentage of soil, ground recycled concrete powder and neutral water was established in a 4:1:1 ratio. These percentages were defined according to the drop test of the wet mixture and the morphology of an impacted ball sample. The mixtures with brittle behavior were discarded and the proportion close to the middle range of plastic behavior was selected.

The components were mixed manually in a container until a homogeneous mixture was obtained. Subsequently, the mixture was poured into a rectangular parallelepiped-shaped steel mold with a lid; this device made it possible to produce large blocks in compression by a manual hydraulic pressing in two step of ultimate pressure of 3000 kgf/cm^2 according to the hydraulic pressure gauge. The CEBs were manufactured by quasi-static compression in wet state and maximum compaction pressure was performed with dwelling time of 30 s before performing the second compaction step. The hydraulic pressure applied for the resulting compaction pressure after the second step was 2000 kgf/cm^2 with dwelling time of 2 min in order to slowly release the residual water. The dimensions of the block were 16 mm thick, 38 mm wide and 150 mm long. After the drying stage at room temperature in the laboratory for 28 days, the CEBs were cut with circular saw to produce compression specimens for mechanical testing. Finally, the specimens were tested for compressive strength and three-point flexural strength based on ASTM C 39 and ASTM C 293.

2.2. Experimental tests: uniaxial compression and three-point bending

The required properties to evaluate the performance of the blocks are obtained from compressive strength test and three-point flexural strength test based on ASTM C 39 and ASTM C 293, respectively. An Instron 3369 universal testing machine with maximum load of 50 kN for

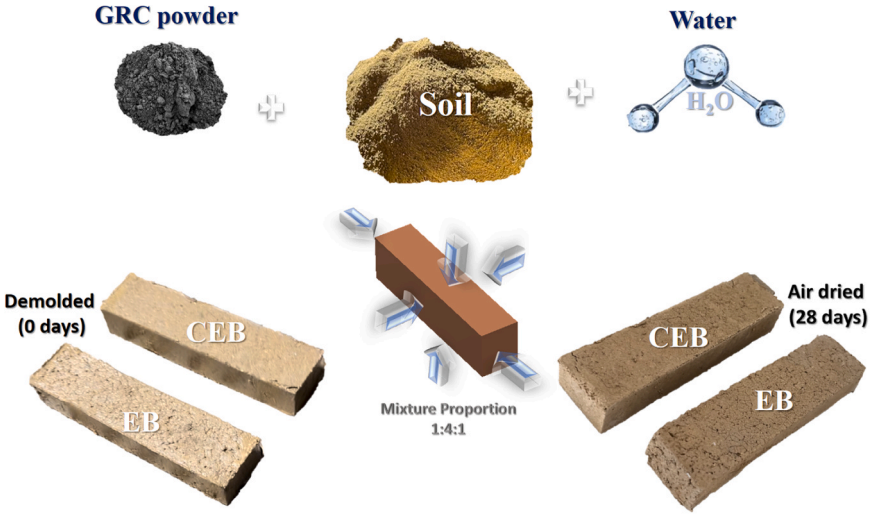

Fig. 1. Constituents, proportions and stages for CEBs manufacturing.

both test is used (Fig. 2). The displacement velocity control for compression test was set at 1 mm/min while for bending test the machine was load rate controlled with 0.3 kN/min. The samples dimensions for bending were 38 mm height, 16 mm depth, total length of 150 mm. The compression block specimen dimensions were 19 mm width, 26 mm depth and 39 mm height. For three-point bending, the block was placed with its greatest transverse length in the direction of the center load and on two rigid steel supports spaced at a distance of 100 mm from each end. The load was applied at the center of the block until complete fracture. The maximum applied load was 230 N. For compression tests, two steel plates (50 mm thick) were placed one above and one below the block in the universal testing machine. A maximum load of 1.2 kN was reach until initial failure of the samples. Three samples per each type of tests were considered.

2.3. SEM-EDS analysis

The identification and quantification of the elements present in the CEB sample was performed by SEM-EDS analysis. This method also allows to determine qualitatively the chemical composition and morphological structure of the as-manufactured CEB samples, as well as to perform analysis of failure mechanism of the CEB under the tensile and compressive stress state. The results from the spectra and element distribution maps, indicate that the matrix of the soil sample includes mineral fractions that are organized in three-dimensional structures. According to the SEM images, the CEB matrix is observed to be heterogeneous, including SEM-visible porous and granular structure.

2.4. Computation of material properties

For compression, the axial stress is obtained from the load (F) and the current cross-section area (A) of the sample ($\sigma = F/A$). As the applied axial displacement during loading is length dependent for an objective unit of deformation, normalized strain from lengthening of the sample of length l considering an infinitesimal incremental length dl provides the definition of infinitesimal strain as $d\varepsilon = dl/l$. Integrating this basic local strain definition between the initial gauge length (lo) and current length (l), and assuming uniform deformation we obtain $\varepsilon = \ln(l/lo)$, or $\varepsilon = \ln(1 + \Delta l/lo) = \ln(1 + e)$, being e the commonly used engineering strain definition. The mathematical expression of ε in the expanded form using Taylor polynomials is $e - e^2/2 + e^2/2 + \ldots e^n/n$, and considering that for quasi-brittle materials the strain range during loading are generally small < 0.05, one can neglect the superior order terms, from which the objective definition of strain becomes $\varepsilon \approx e$ (Eq. 1) and stress definition for small strains is now justified and given in Eq. 2:

$$\varepsilon = \ln\left(\frac{l}{lo}\right) \approx e = \frac{\Delta l}{lo};\ \ \varepsilon < 0.05 \tag{1}$$

$$\sigma = \frac{F}{Ao}; for\ \varepsilon < 0.05 \tag{2}$$

For the calculation of strain in symmetric brittle beam under central transverse load, called here the well-known three-point bending testing, one can assume that the applied transversal displacement in the center of the beam produces an incremental lengthening and shortening $d\delta$ of an infinitesimal beam proportion dl in the axial axis. Assuming that the small deflection of the beam in the centroid axis is a circular arc of radius R, and cross-sectional plane remains plane during deformation, the infinitesimal angle is $d\varnothing = dl/R = (dl + d\delta)/(R + h/2)$, with h the height of the beam. Rearranging the two last equivalent terms, one can obtain $h/2R = d\delta/dl$. The latter is the engineering strain definition in the axial direction of the beam, and considering uniform deformation in the axial or longitudinal coordinate (uniform circular arc), the axial strain (e) can therefore be calculated from the instant applied transversal displacement (δ) times the distance between the two lower supports of the beam (L). Assuming the linear relation of stress (σ) with strain, as well as the equivalence between bending moment acting on the cross-section and the sum of differential bending moment produced from the local values of stress applied in a differential area located at a certain distance from the centroid axis, the maximum value of σ at the free lower (tensile) and upper surface (compression) is computed. Besides, neglecting the asymmetrical stress-strain relations from tensile and compression behavior, the Flexural modulus (E) is also obtained.

3. Results and discussion

In this section, the processed data from the laboratory tests and the results of the proposed and calibrated nonlinear model are presented. Compressive force versus axial displacement and bending forces versus displacement curves in elastic, maximum strength and damage regime are compared and examined for the two type of earth blocks. In addition, failure modes, crack propagation and microcracks are analyzed using SEM data. CEBs, as other quasi-brittle granular materials, have a differential behavior in tension and compression (SD effect). This mechanical behavior is well reproduced by a mathematical model that is provided and calibrated for elasticity and loss of load capacity due to damage and cracks.

3.1. Stress-strain under compression load

As shown in Fig. 3a, for the experimental CEB specimen loaded by an axial force of compression, the load increases progressively with deformation until reaching a maximum strength value of approximately 2.4 MPa and with an axial displacement of approximately 0.61 mm. Note that the maximum stress value reached is not comparable with other CEBs obtained by testing method using a low height/width ratio as

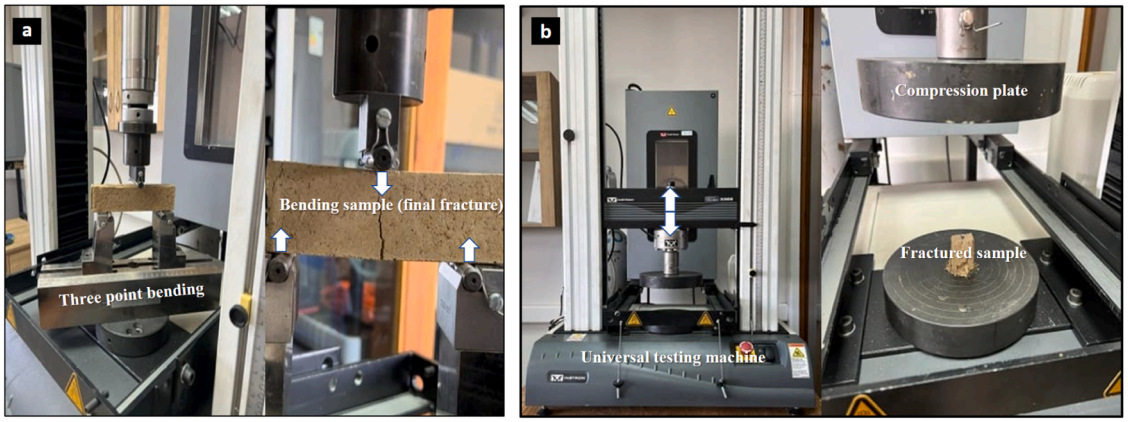

Fig. 2. Experimental mechanical testing of CEB samples using a universal machine. Set up for (a) flexural test and (b) compression testing.

a triaxial stress state appears instead of uniaxial. The behavior investigated here is uniaxial, so assuring a minimum value of 2 for height/width ratio is required. The strain at maximum stress is 0.0094, while the maximum strain experienced by the material at the proportional limit in response to the applied compressive load is 0.003. On the other hand, the maximum value of load that the material sample can withstand before failure is 1204 N. The increase in stress with strain as seen in Fig. 3 is almost linear and could be described by a Hook's law. However, a more accurate model including the nonlinear macroscopic observed behavior is also targeted. Note that axial stress is calculated with load and initial cross-section of the sample. This is valid for non-damaged sample, however, as its shown in Fig. 3, samples with cracks presents a reduced cross-sectional area to resist the load. This reduced area resisting the applied load is subjected to higher stress than the stress value computed with the initial cross-section of the earth material. This is valid for both, bending and compression loading.

At maximum load resistance, the computed macroscopic stress in the samples is non linearly reduced. This behavior is generally called softening of the material. Tensile stresses induced in the sample by bending show a rapid decrease with the strain applied in comparison to compression sample. This phenomenon should be included in the mathematical modeling.

3.2. Stress-strain from flexural load

The maximum load that the material can withstand before fracturing under bending loads for the tested CEB prism is 231 N, which is equivalent to a maximum bending tensile stress value of 0.858 MPa (Fig. 3b). Compared to the EB tested with a maximum tensile stress of 0.53 MPa and extruded soil blocks reported in the literature with similar characteristics [26,27], CEB proves to exhibit superior strength as expected. Note that calculated stress value in bending is equivalent to the maximum stress reached under uniaxial tensile deformation. The difference relies on the proportion of material in the homogeneous stress state, which in conventional tensile testing is the entire cross-section. As for bending, only a line of material where the maximum stress occurs can be considered uniaxial. This is because in the upper and lower free surface of the material there is no shear stress, causing the stress and strain state to be equivalent to the tensile stress. The figure also shows that the strain exhibited by the CEB prism at the maximum stress value is 0.55%. Subsequently, the damage of the material begins to be seen in the material curve, showing a drastic drop. Note that the rate of decrease of stress as a function of strain may be further accentuated by the considerations made in the derivation of the mathematical equation governing the calculation of maximum stress in the beam and applied to compute the macromechanical experimental stress in the damage zone of the graph in Fig. 3b.

3.3. Modeling of strength and damage of quasi-brittle CEBs

The compressive behavior of CEB is fully modeled using the nonlinear stress-strain relationship expressed mathematically in a rising-descending curve (Eq. 3). Fig. 4b shows the experimental and model-defined axial stress-strain-compression curves calibrated with a mean average percentage error (MAPE) of 4%. The model is fully dependent of only two material parameters, the stress-strain point at maximum uniaxial compression stress $(\varepsilon_{\max}, \sigma_{\max})$, and a softening-damage parameter $n > 1$ given in Fig. 4b.

$$\sigma = \sigma_{\max} \frac{n\left(\frac{\varepsilon}{\varepsilon_{\max}}\right)}{(n-1) + \left(\frac{\varepsilon}{\varepsilon_{\max}}\right)^n} \tag{3}$$

Note that in building construction, the force in soil blocks is multiaxial. The experimental data needed to calibrate the mathematical model are uniaxial. If multiaxial compression data are available, a finite element simulation is required for computing the stress tensor with the corresponding hydrostatic and deviatoric components. From the deviatoric stress, using the equivalent Mohr–Coulomb (M&C) stress, the value of the maximum stress can be calculated to calibrate to the mathematical model.

In the case of tensile stress state, the observed behavior is significantly different. The linear material behavior in the elastic regime until the maximum tensile stress is modeled using a classical Hook's law. After the peak, incremental deformation produced by increase of load are described by the exponential equation depending inversely from the increase of strain (Eq. 4). The *m*-value model the rate at which the material softens due to damage. The calibrated phenomenological damage model depicted in Fig. 4a slightly overestimate the stress capacity, with an average accuracy of stress prediction of 62%. This value is neglected as non-representative prediction capacity due to the nature of the stress-strain response. High value of stress slope forces to define the prediction accuracy or calibration error in terms of strains at similar compared stress value. In this sense, a prediction accuracy of 96.8% (MAPE of 3.2) is achieved.

$$\sigma = \sigma_{\max} \left(\frac{\varepsilon_{\max}}{\varepsilon}\right)^m \tag{4}$$

Stress states and fracture morphology are examined to analyze the failure mechanism of the EB and CEB materials. For earth and mineral materials, the failure mechanism observed is generally called brittle cleavage failure, with smooth specific failure planes well defined. Another feature of fracture is that as brittle material; ultimate compressive strength is much higher than the ultimate tensile strength. According to Barsanescu et al. [28] this behavior affecting the strength of the material may also be due to the presence of porosities and

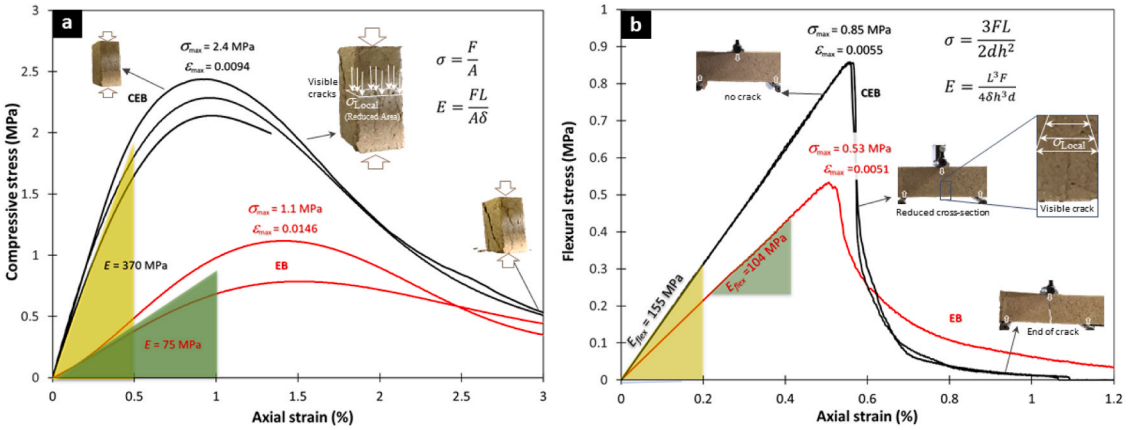

Fig. 3. Testing results of CEBs and EB: (a) compression and (b) three-point bending.

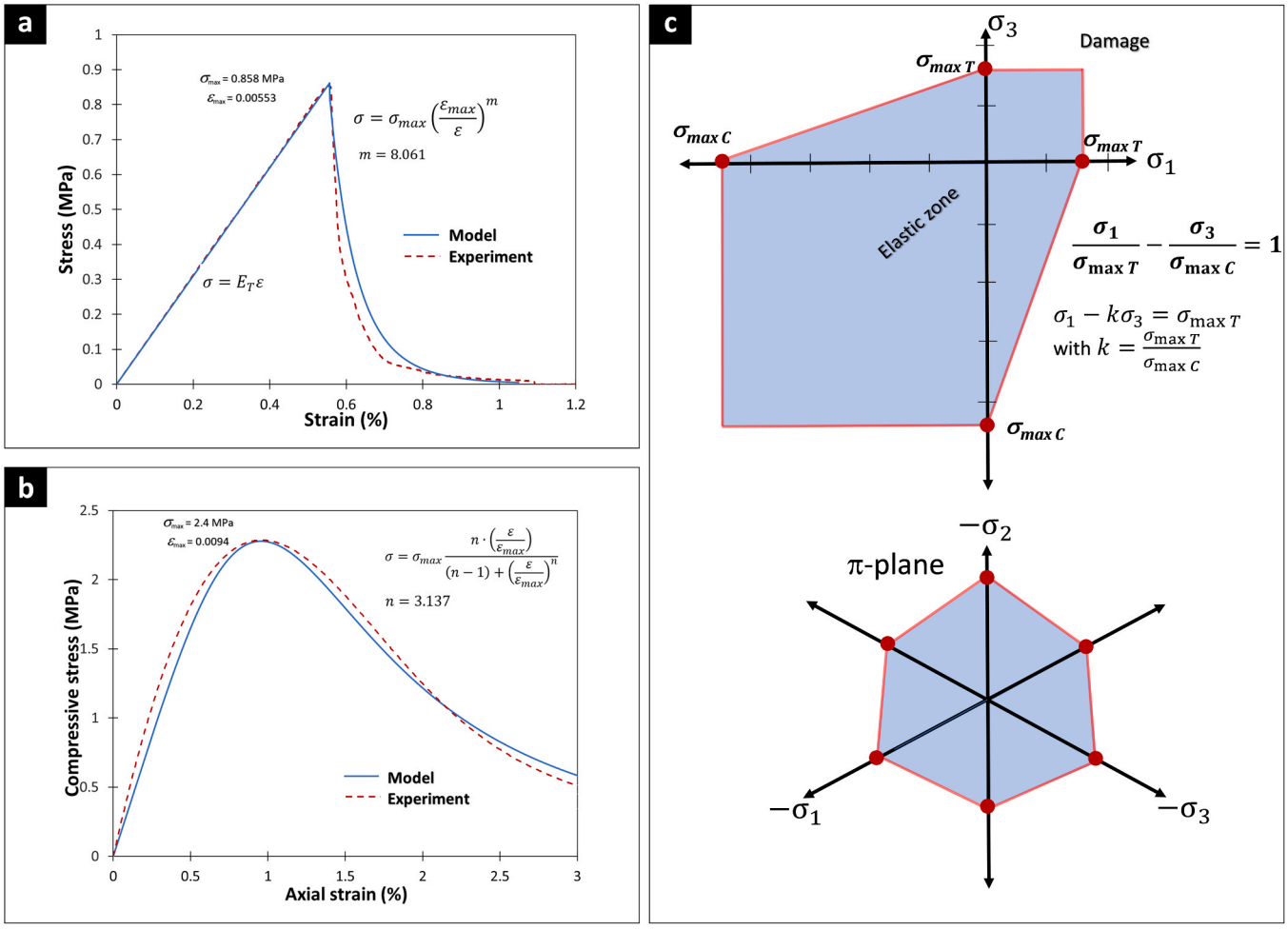

Fig. 4. Prediction of the calibrated mathematical model for CEB under (a) tension and (b) compression. (c) The failure limit is given according to a M&C criterion considering the tension-compression asymmetry.

microcracks in the CEB. The tensile strength test of the block shows the mechanism of crack formation and subsequent propagation and widening. In the initial process, a microcrack is generated and with further loading, these microcracks propagate and unite to form macro-cracks. The growth and propagation of these micro-cracks contributes to the non-linear macroscopic stress-strain behavior and plastic deformation of the material. The stress concentrators or maximum material bonding stress located in the crack lead to this propagation and final fracture of the material.

The classical failure criterion of maximum combined stress in brittle materials proposed by Mohr–Coulomb (M&C) is selected to analyze the safe elastic limit and damage propagation in the CEB. M&C failure criterion is a hexagonal pyramid with the tip on the positive side of the hydrostatic axis. The cross section in the deviatoric stress plane is an irregular hexagon (Fig. 4c). Some of the advantages of the Mohr–Coulomb failure criterion are related to the fact that it is widely used for brittle isotropic materials (such as rocks or concrete, etc.). These materials have asymmetric response in terms of tensile and compression stress-strain relationship, generally called strength differential effect (SD) [28,29]. Another more complex emerging SD failure criterion is for anisotropic material, called CPB06. This model includes an anisotropic matrix with several materials parameters, which requires a larger number of testing data but provides a more accurate representation of the failure limit in complex materials [30,31]. Fig. 4c shows the mathematical expression for the failure limit adopted in the major and minimum principal stress plane (σ_1-σ_3). In addition to the softening-damage models, a combined directional equivalent stress may be computed from Eq. 5.

$$\sigma_{M\&C} = \begin{cases} \sigma_{maxT}\left(\dfrac{\varepsilon_{maxT}}{\varepsilon}\right)^m & ;\sigma_1 \text{ or } \sigma_3 > \sigma_{maxT} \\ \sigma_{maxC}\dfrac{n\left(\frac{\varepsilon}{\varepsilon_{max\,C}}\right)}{(n-1)+\left(\frac{\varepsilon}{\varepsilon_{maxC}}\right)^n} & ;\sigma_1 \text{ or } \sigma_3 < \sigma_{maxC} \\ \sigma_{maxT} + k\sigma_{maxC}\dfrac{n\left(\frac{\varepsilon}{\varepsilon_{maxC}}\right)}{(n-1)+\left(\frac{\varepsilon}{\varepsilon_{maxC}}\right)^n} & \sigma_1 - k\sigma_3 > \sigma_{maxT} \end{cases} \quad (5)$$

3.4. Microstructural features of soil and CEBs via SEM/EDS analysis

In this study, the microstructural characteristics of the soil and earthen block materials are performed using the scanning electron microscope (SEM). The SEM allows obtaining magnified images of the shape, size, composition, crystallography and other physical and chemical properties of a sample. On the other hand, the elemental composition, as part of this study, is determined by energy dispersive X-ray spectrometer (EDS) to obtain an elemental mapping and a localized chemical analysis, allowing to analyze the samples quantitatively and qualitatively.

From Figs. 5b and 5c, the point elemental chemical composition R1, R2 and R3 of the selected zone is observed at x500 magnification. The cementitious particles are observed as small whitish spheroidal particles

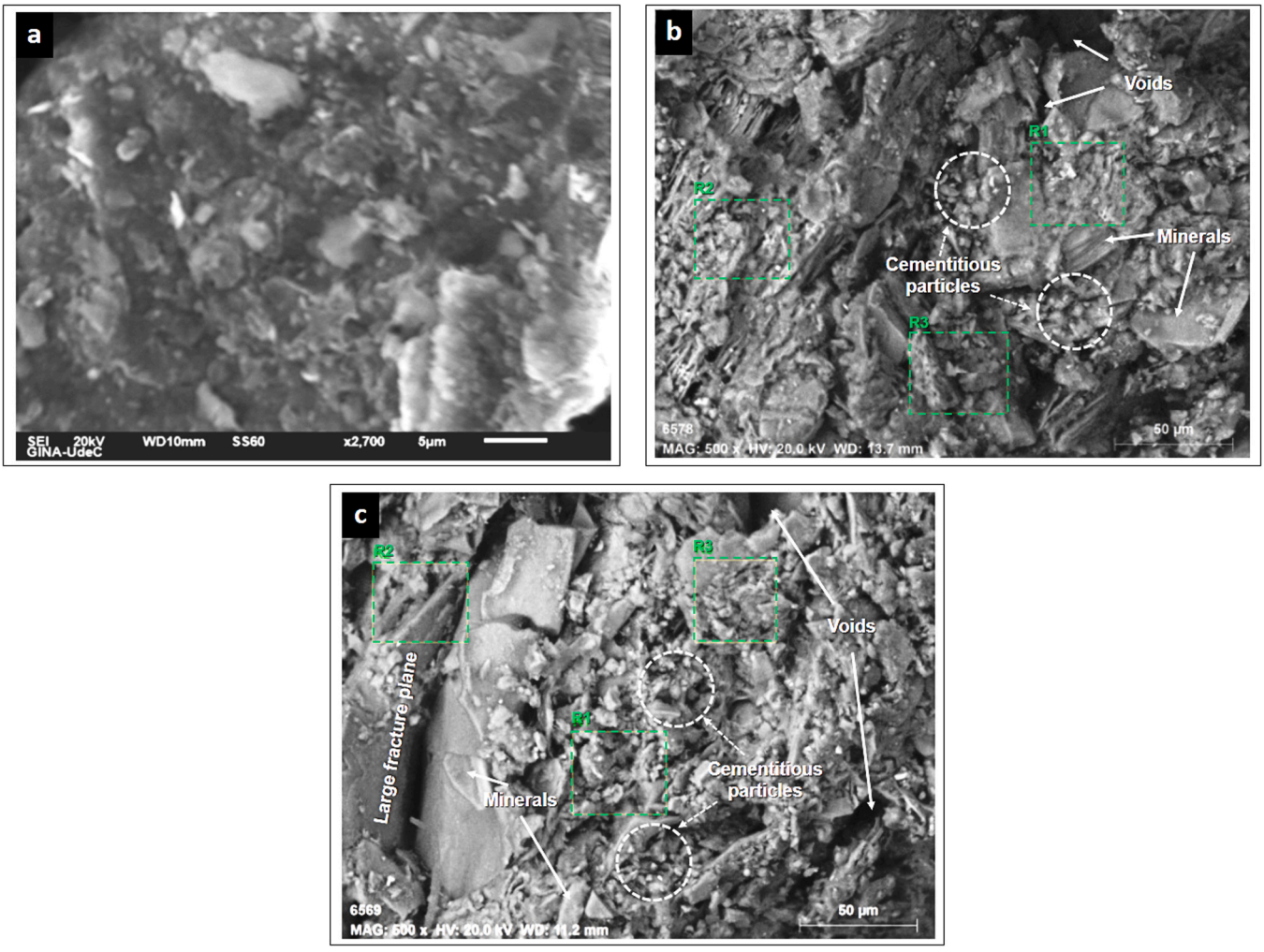

Fig. 5. SEM observations of the (a) soil, and fracture plane from compression testing samples (b) CEB and (c) EB.

attached to the soil minerals. The recycled cement powder provides these calcium-based minerals, which is evidenced in Fig. 5b (CEB SEM) by the presence of Ca elements and Na elements (Fig. 6b). During manufacture, it is expected that calcium silicate hydrate or calcium aluminate hydrate will be formed by the reaction between water and recycled cement powder arranged around the particles. The figure also clearly shows minerals of different shapes and sizes, mainly from the soil used. The most representative mineral forms are observed as laminated or layered structures typical of phyllosilicate minerals. In Fig. 5b, R3 shows more Ca than R1 and R2. Finally, Fig. 6a shows the spectrum of the soil used; where the presence of Ca and Na elements is not observed, unlike the spectra of Figs. 6b and 6c that include these elements due to the incorporation of recycled cement powder (GRC). Spheroidal cementitious particles derive from GRC show to provide higher particle cohesion and consequent material strength. This is proved by comparing SEM images of aforementioned Figs. 5b and 5c. In CEB region of interest with highly smashed zones (R1 in Fig. 5b) low values of Na and Ca are found while, in last local fractures region with no local plastic deformation (R3 in Fig. 5b) higher values of Na and Ca are shown by EDS analysis (Fig. 6b). In case of EB, comparing the local values in the marked micro-crack zone on the fracture plane (R2), the low Ca contents shown by the EDS analysis (Fig. 6c) are associated with lower strength and primary occurring cracks.

Fractography analysis of CEBs via SEM indicates that the microstructure contains several micro voids and cracks, particularly at the interfaces between the coarse GRCs and soil grains (Fig. 5b). These initial voids and cracks are generally due to shrinkage during curing. The defects observed in SEM images of the postmortem specimen are detected here in the fracture planes after the compressive load is applied. As stronger bond between the particles is required to increase material strength, this can be achieved by adding smaller particles or reduce spacing by functional binder particles such as Portland cement.

To understand the macromechanical behavior of SD effect, the dissimilar damage and relatively ductile compressive and brittle tensile behavior (Fig. 4a and Fig. 4b), the correlation with microstructural fracture characteristics of SEM images explains that low tensile strength and softening from damage and fracture mechanism due to weakening of interparticle bond drives a brittle tensile behavior; while the higher strength and ductile compression observed are due to the occurrence of micro-cracks and the growth of cracks and friction between fracture planes from coarse and hard grains. Note that similar behavior is for both materials, CEB (Fig. 5b) and EB (Fig. 5c) in terms of brittle and ductile tensile-compression asymmetric behavior; while the lower EB strength is explained from its observed fracture surface presenting larger developed planes of micro-cracks during loadings. Additional work is further required as the proposed mathematical models of Section 3.3 do not provide the necessary data to perform a deeper analysis of the macro/micro fracture morphology. For this purpose, a model based on micromechanics of porous materials, such as SC11–TNT [29] or the coupled theory of phase field and plasticity [32] should be investigated and evaluated.

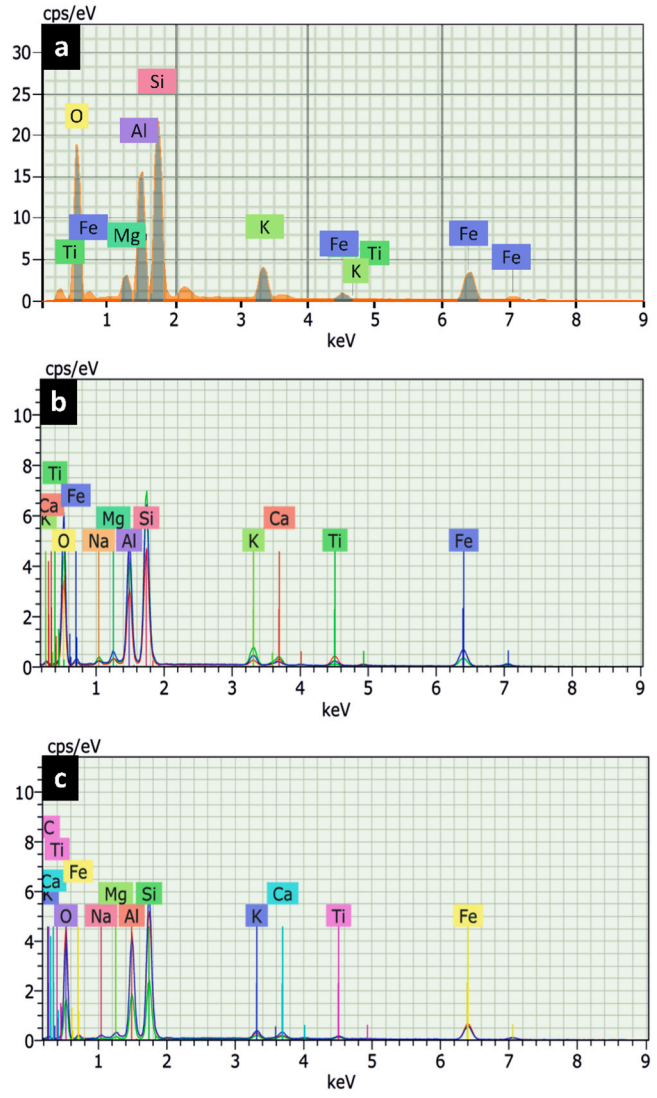

Fig. 6. EDS of (a) soil, and compression fracture planes of (b) CEB and (c) EB.

4. Conclusions

In this study, the microstructure and macromechanical behavior of quasi-brittle manufactured earth blocks (EB) and compressed earth blocks (CEB) was determine using compression testing, three-point bending and SEM-EDS analysis. A mathematical model describing the observed strength-deformation behavior, hardening and damage induced softening was proposed and accurately calibrated. The directional evolution of the failure limit in terms of M&C criterion was also included to account the strong SD effect. According to the analysis of results, the following general conclusions are given:

- The macromechanical behavior of SD effect, dissimilar damage and the relatively ductile compressive and brittle tensile behavior are derived from microstructural features of localized fracture zones; with lower tensile strength and brittle fracture due to weakening damage mechanism of interparticle bonding, and higher strength and more ductile compressive behavior from micro-cracks onset and cracks development limited by friction between fracture planes from coarse and hard grains.
- The superior strength of CEB compared to EB is associated to higher compaction pressure, which reduces voids, and increases particle cohesions and interactions, promoting the formation of cementitious materials from ground recycled concrete powder. Compaction during CEB manufacturing increases strength by reducing size of micro-cracks planes development during compressive loadings.
- The compressive behavior of CEBs was successfully modeled using a nonlinear stress-strain relationship, expressed mathematically in a rising-descending curve. The model showed good agreement with experimental results, with a mean average percentage error (MAPE) of 4%. The model is fully dependent on two material parameters, namely the stress-strain point at maximum uniaxial compression stress (ε_{max}, σ_{max}) and a softening-damage parameter ($n > 1$).
- The tensile behavior of CEBs was modeled using a combination of classical Hook's law in the elastic regime and an exponential equation after the peak stress point to capture softening due to damage. The calibrated phenomenological damage model slightly overestimated the stress capacity, but overall, it achieved a high prediction accuracy of 96.8% (MAPE of 3.2) in terms of strains at similar compared stress values.
- The fracture analysis of CEBs reveals the presence of microvoids and cracks, especially at the interfaces between coarse particles and soil grains. Our study suggests that the brittle behavior observed in tension for CEBs is attributed to the weakening of inter-particle bonds, leading to higher susceptibility to fracture under tensile stresses. On the other hand, the ductile compressive behavior of CEBs is influenced by the presence of microcracks and friction between the fracture planes of coarse and hard particles, which restricts crack propagation and contributes to a more robust compressive strength.

Additional effort is required for the numerical implementation of the proposed CEB model in a finite element code. Moreover, for an accurate simulation of strength in walls and buildings, the evaluation and validation of the predicted response of the blocks under biaxial, triaxial/confined compression and direct shear tests is required.

CRediT authorship contribution statement

Marian Valenzuela: Conceptualization, Methodology, Formal analysis, Investigation, Resources, Validation, Funding acquisition, Data curation, Visualization, Writing - original draft, Writing - review & editing. **Jorge Leiva:** Resources, Investigation. **Alexis Salas:** Resources. **Gustavo Ciudad:** Supervision, Funding acquisition. **Juan Pablo Cárdenas:** Resources. **Angelo Oñate:** Writing – review & editing. **Renato Hunter:** Resources. **Shady Attia:** Writing – review & editing. **Víctor Tuninetti:** Investigation, Funding acquisition, Project administration, Resources, Writing – review & editing.

Declaration of Competing Interest

The authors declare that they have no known competing financial interests or personal relationships that could have appeared to influence the work reported in this paper.

Data availability

The data that support the findings of this study are available from the corresponding authors upon reasonable request.

Acknowledgments

The authors would like to thank the ANID Doctorado Nacional 2022-21222107 for the financial support of this research under the PhD postgraduate scholarship of Marian Valenzuela. Acknowledgements are also included for the help of different internal units of the Universidad de La Frontera such as IMA, BIOREN under Fondequip EQM170220, Construction Laboratory under Fondecyt 1180414 and Composite Materials Laboratory under Fondequip EQM180111.

References

[1] C. Turco, A.C. Paula Junior, E.R. Teixeira, R. Mateus, Optimisation of Compressed Earth Blocks (CEBs) using natural origin materials: a systematic literature review, Constr. Build. Mater. (2021), https://doi.org/10.1016/j.conbuildmat.2021.125140.

[2] A. Jesudass, V. Gayathri, R. Geethan, M. Gobirajan, M. Venkatesh, Earthen blocks with natural fibres - a review, Mater. Today Proc. 45 (2020) 6979–6986, https://doi.org/10.1016/j.matpr.2021.01.434.

[3] A. Laborel-Préneron, J.E. Aubert, C. Magniont, C. Tribout, A. Bertron, Plant aggregates and fibers in earth construction materials: a review, Constr. Build. Mater. 111 (2016) 719–734, https://doi.org/10.1016/j.conbuildmat.2016.02.119.

[4] N. Jannat, A. Hussien, B. Abdullah, A. Cotgrave, Application of agro and non-agro waste materials for unfired earth blocks construction: a review, Constr. Build. Mater. 254 (2020), 119346, https://doi.org/10.1016/j.conbuildmat.2020.119346.

[5] P. Nshimiyimana, H.S. Moussa, A. Messan, L. Courard, Effect of production and curing conditions on the performance of stabilized compressed earth blocks: kaolinite vs quartz-rich earthen material, MRS Adv. (2020), https://doi.org/10.1557/adv.2020.155.

[6] A.L. Murmu, A. Patel, Towards sustainable bricks production: an overview, Constr. Build. Mater. 165 (2018) 112–125, https://doi.org/10.1016/j.conbuildmat.2018.01.038.

[7] M. Yatawara, S. Athukorala, Potential of replacing clay soil by rice husk ash (RHA) in enhancing the properties of compressed earth blocks (CEBs), Environ. Dev. Sustain. 23 (2021) 3474–3486, https://doi.org/10.1007/s10668-020-00727-9.

[8] M. Sassu, A. Romanazzi, L. Giresini, W. Franco, C. Ferraresi, G. Quaglia, E. Orefice, Production procedures and mechanical behaviour of interlocking stabilized compressed earth blocks (ISCEBs) manufactured using float ram 1.0 press, Eng. Solid Mech. (2018) 89–104, https://doi.org/10.5267/j.esm.2018.3.004.

[9] S.N. Malkanthi, W.G.S. Wickramasinghe, A.A.D.A.J. Perera, Use of construction waste to modify soil grading for compressed stabilized earth blocks (CSEB) production, Case Stud. Constr. Mater. 15 (2021), e00717, https://doi.org/10.1016/j.cscm.2021.e00717.

[10] P. Kasinikota, D.D. Tripura, Prediction of physical-mechanical properties of hollow interlocking compressed unstabilized and stabilized earth blocks at different moisture conditions using ultrasonic pulse velocity, J. Build. Eng. 48 (2022), 103961, https://doi.org/10.1016/j.jobe.2021.103961.

[11] C.A. Oyelami, J.L.Van Rooy, A review of the use of lateritic soils in the construction/development of sustainable housing in Africa: a geological perspective, J. Afr. Earth Sci. 119 (2016) 226–237, https://doi.org/10.1016/j.jafrearsci.2016.03.018.

[12] O.B. Adegun, Y.M.D. Adedeji, Review of economic and environmental benefits of earthen materials for housing in Africa, Front. Archit. Res. (2017), https://doi.org/10.1016/j.foar.2017.08.003.

[13] P.M. Touré, V. Sambou, M. Faye, A. Thiam, M. Adj, D. Azilinon, Mechanical and hygrothermal properties of compressed stabilized earth bricks (CSEB), J. Build. Eng. 13 (2017) 266–271, https://doi.org/10.1016/j.jobe.2017.08.012.

[14] O. Izemmouren, A. Guettala, S. Guettala, Mechanical properties and durability of lime and natural pozzolana stabilized steam-cured compressed earth block bricks, Geotech. Geol. Eng. 33 (2015) 1321–1333, https://doi.org/10.1007/s10706-015-9904-6.

[15] H. Danso, D.B. Martinson, M. Ali, J.B. Williams, Physical, mechanical and durability properties of soil building blocks reinforced with natural fibres, Constr. Build. Mater. 101 (2015) 797–809, https://doi.org/10.1016/j.conbuildmat.2015.10.069.

[16] J.M. de Souza, R.E.B. Ramos Filho, J.B. Duarte, V.M. da Silva, S.R. do Rêgo, L. de, F.L. Lucena, W. Acchar, Mechanical and durability properties of compressed stabilized earth brick produced with cassava wastewater, J. Build. Eng. 44 (2021), https://doi.org/10.1016/j.jobe.2021.103290.

[17] Y. Labiad, A. Meddah, M. Beddar, Physical and mechanical behavior of cement-stabilized compressed earth blocks reinforced by sisal fibers, Mater. Today Proc. 53 (2022) 139–143, https://doi.org/10.1016/j.matpr.2021.12.446.

[18] T. Mohamed, A. Hajar, E. Hassan, F. M'bark, Thermal, mechanical and physical behavior of compressed earth blocks loads by natural wastes, Int. J. Civ. Eng. Technol. (2018).

[19] H. Wu, C. Liang, Z. Zhang, P. Yao, C. Wang, Z. Ma, Utilizing heat treatment for making low-quality recycled aggregate into enhanced recycled aggregate, recycled cement and their fully recycled concrete, Constr. Build. Mater. 394 (2023), 132126, https://doi.org/10.1016/j.conbuildmat.2023.132126.

[20] C. Shi, Y. Li, J. Zhang, W. Li, L. Chong, Z. Xie, Performance enhancement of recycled concrete aggregate – a review, J. Clean. Prod. 112 (2016) 466–472, https://doi.org/10.1016/j.jclepro.2015.08.057.

[21] W. Bai, J. Shen, J. Guan, J. Wang, C. Yuan, Study on compressive mechanical properties of recycled aggregate concrete with silica fume at different strain rates, Mater. Today Commun. 31 (2022), 103444, https://doi.org/10.1016/j.mtcomm.2022.103444.

[22] Y. Kaya, B. Aytekin, T. Kaya, A. Mardani, Investigation of pozzolanic activity of recycled concrete powder: effect of cement fineness, grain size distribution and water/cement ratio, Mater. Today Proc. (2023), https://doi.org/10.1016/j.matpr.2023.03.137.

[23] J. Kim, N. Nciri, A. Sicakova, N. Kim, Characteristics of waste concrete powders from multi-recycled coarse aggregate concrete and their effects as cement replacements, Constr. Build. Mater. 398 (2023), 132525, https://doi.org/10.1016/j.conbuildmat.2023.132525.

[24] B. Cantero, M. Bravo, J. de Brito, I.F. Sáez del Bosque, C. Medina, Water transport and shrinkage in concrete made with ground recycled concrete-additioned cement and mixed recycled aggregate, Cem. Concr. Compos. 118 (2021), https://doi.org/10.1016/j.cemconcomp.2021.103957.

[25] B. Cantero, M. Bravo, J. de Brito, I.F. Sáez del Bosque, C. Medina, Mechanical behaviour of structural concrete with ground recycled concrete cement and mixed recycled aggregate, J. Clean. Prod. 275 (2020), 122913, https://doi.org/10.1016/j.jclepro.2020.122913.

[26] P. Muñoz, V. Letelier, L. Muñoz, D. Zamora, Assessment of technological performance of extruded earth block by adding bottom biomass ashes, J. Build. Eng. 39 (2021), https://doi.org/10.1016/j.jobe.2021.102278.

[27] R. Abid, N. Kamoun, F. Jamoussi, H. El Feki, Fabrication and properties of compressed earth brick from local Tunisian raw materials, Bol. La Soc. Esp. Ceram. Y. Vidr. 61 (2022) 397–407, https://doi.org/10.1016/j.bsecv.2021.02.001.

[28] P. Barsanescu, A. Sandovici, A. Serban, Mohr-Coulomb criterion with circular failure envelope, extended to materials with strength-differential effect, Mater. Des. 148 (2018) 49–70, https://doi.org/10.1016/j.matdes.2018.03.043.

[29] C. Rojas-Ulloa, V. Tuninetti, H. Sepúlveda, E. Betaieb, G. Pincheira, G. Gilles, L. Duchêne, A.M. Habraken, Accurate numerical prediction of ductile fracture and micromechanical damage evolution for Ti6Al4V alloy, Comput. Mech. (2023), https://doi.org/10.1007/s00466-023-02362-3.

[30] V. Tuninetti, G. Gilles, P. Flores, G. Pincheira, L. Duchêne, A.-M. Habraken, Impact of distortional hardening and the strength differential effect on the prediction of large deformation behavior of the Ti6Al4V alloy, Meccanica 54 (2019) 1823–1840, https://doi.org/10.1007/s11012-019-01051-x.

[31] C. Rojas-Ulloa, C. Bouffioux, A.F. Jaramillo, C.M. García-Herrera, T. Hussain, L. Duchêne, G. Riu, J. Josep Roa, P. Flores, A. Marie Habraken, V. Tuninetti, Nanomechanical characterization of the deformation response of orthotropic Ti–6Al–4V, Adv. Eng. Mater. 23 (2021) 2001341, https://doi.org/10.1002/adem.202001341.

[32] J. Choo, W. Sun, Coupled phase-field and plasticity modeling of geological materials: from brittle fracture to ductile flow, Comput. Methods Appl. Mech. Eng. 330 (2018) 1–32, https://doi.org/10.1016/j.cma.2017.10.009.